A&A manuscript no.
(will be inserted by hand later)

Your thesaurus codes are:
05.03.1; 07.13.2

ASTRONOMY
AND
ASTROPHYSICS
14.8.2000

Direct solar radiation pressure on the orbits of small near–Earth asteroids: Observable effects?

David Vokrouhlický[1] and Andrea Milani[2]

[1] Institute of Astronomy, Charles University, V Holešovičkách 2, CZ-180 00 Prague 8, Czech Republic
[2] Dipartimento di Matematica, Università di Pisa, Via Buonarotti 2, I-56127 Pisa, Italy
(Electronic addresses: vokrouhl@mbox.cesnet.cz, milani@dm.unipi.it)

August 14, 2000

Abstract. We consider the perturbations of Near–Earth Asteroid orbits due to direct solar radiation pressure (both the absorption and the reflection components). When the body is spherical and the surface albedo homogeneous the effect is small (and only short–periodic). However, when at least one of these restrictive and unrealistic assumptions is relaxed, long–term orbital effects appear and they may potentially lead to observable displacement of the orbit. We illustrate this conclusion by computing the orbital perturbations due to radiation pressure for objects with an odd–zonal distribution of albedo and for objects with ellipsoidal shape. Especially in the first case the effects are large, due to the long–term perturbations of the semimajor axis. For high–eccentricity orbits observed over a long interval of time, the (v/c)–correction of the direct radiation pressure, known as Poynting–Robertson effect, should be also considered. As an example we demonstrate that for the asteroids 6489 Golevka and 1566 Icarus, during their next close approach to the Earth, the orbit displacement due to the direct solar radiation forces might be, under reasonable assumptions, comparable to the orbit determination uncertainty, thus potentially observable.

Key words: Celestial mechanics – Minor planets, asteroids – Meteoroids

1. Introduction

Tiny non–gravitational effects may become important in the dynamics of the cosmic bodies provided one (or both) of the following two circumstances are satisfied: (i) orbital data of a superb quality are available, and/or (ii) the effect leads to long–term perturbations accumulating over long time span. This is also the case of radiation forces acting on orbits of natural and artificial cosmic bodies.

Radiation force effects in the motion of the Moon represent an outstanding example of the above mentioned case (i). The lunar motion data acquired through the laser ranging to the surface retroreflectors achieved a centimeter precision in the mid nineties, an unprecedented quality among the orbital data of a natural body. Vokrouhlický (1997) showed that the radiation forces due to the absorbed, reflected and thermally re–processed sunlight cause a synodic oscillation of the lunar geocentric distance of about 4 millimeters, a statistically important value given the data precision (see, e.g., Williams et al. 1996). The motion of solar system dust particles, either interplanetary or circumplanetary, is a good example of the applicability of (ii). In this case we do not have data about the individual orbits, but we may determine statistical properties of a large ensemble of such particles (such as the location and extension of the dust bands). These data may be then matched with orbital histories undergoing a long–term (or secular) effects due to the Poynting–Robertson and other effects. At somewhat larger sizes, the Yarkovsky effect, a radiation recoil force due to the thermally reemitted sunlight, takes the role of the Poynting–Robertson effect. Certain physical properties of meteorites (like the cosmic radiation exposure ages) may indirectly indicate past orbital histories of the meteoroids with an important contribution of the Yarkovsky–effect–dominated phase (Vokrouhlický & Farinella 2000). For the motion of some artificial satellites both assumptions (i) and (ii) may be valid. For instance, the orbits of LAGEOS and other geodynamics satellites are monitored with centimeter precision over decades. This allowed to detect anomalous signals that were later recognized as a signature of various radiation effects acting on orbits of these satellites.

In a recent paper, Vokrouhlický et al. (2000) advocated that the motion of the Near–Earth Asteroids (NEAs) may also represent a problem in which both (i) and (ii) are satisfied. For observations, we have very precise radar data

Send offprint requests to: D. Vokrouhlický for about 50 NEAs, out of which about a dozen have been observed by radar at two close approaches to the Earth. Vokrouhlický et al. (2000) computed the orbit perturbation due to the Yarkovsky effect for selected NEAs and demonstrated that the corresponding perturbations can be observable during their next close approaches to the Earth. A secular change of the semimajor axis was the key feature of the Yarkovsky orbit perturbation.

The goal of this paper is to prove that the so far neglected effect of direct solar radiation pressure (and that of reflected radiation) should be also taken into account, since it can produce large orbit perturbations. These effects were believed by some to be unimportant for the following reasons: (a) the perturbing acceleration is exactly opposed to the gravitational attraction of the Sun and may be modeled by small change in its mass, and (b) NEAs are too large objects. Though (b) is true in many cases, the argument (a) assumes an oversimplified force model, appropriate only for a spherical body with constant surface albedo. None of these two conditions is typically satisfied by the real NEAs. We prove that even the lowest order deviations from spherical shape and/or constant albedo lead to long–term orbital effects. By estimating the order of magnitude of the corresponding perturbations we conclude that these effects might be potentially important for an accurate orbit determination of the NEAs tracked with radar.

To compute with top accuracy the highly eccentric NEAs orbits (like that of Icarus) requires to include also the (v/c)–correction to direct radiation pressure known as Poynting–Robertson (PR) effect (e.g. Burns et al. 1979). At a first sight this seems surprising, since the PR effect is typically associated with the orbital evolution of the dust particles (μm to mm size), while NEAs are macroscopic objects (e.g. Icarus' size is $\simeq 450$ m). However, the secular change in the semimajor axis of the orbit due to the PR effect, appreciably increased by a high eccentricity, results in a quadratic accumulation of the transverse displacement. We argue that for Icarus the PR perturbation largely exceeds the observations uncertainty at the next close approach, though it is somewhat smaller that the orbit determination uncertainty.

The paper is organized as follows: in Sec. 2 we compute the radiation force acting on a spherical asteroid with axially symmetric albedo distribution and the force acting on a ellipsoidal object with constant albedo. We prove that in both cases the orbit undergoes long–term perturbations. The corresponding formulae for the PR effect are recalled. In Sec. 3 we show the expected order of magnitude and character of the orbit perturbation in the case of two precisely known NEA orbits: Golevka and Icarus. Sec. 4 contains some general comments and a discussion of the future prospectives for this kind of research.

2. Theory

Let us consider a body of an arbitrary shape illuminated by solar radiation. The Sun is assumed to be infinitely remote, so that the radiation field consists of parallel light–rays characterized by a unit vector $\mathbf{n}$ ("outward from the Sun"). Denote the geometric cross–section of the body along the direction $\mathbf{n}$ by $P_\perp$. Then, the body's acceleration $\mathbf{a}$ due to the absorbed radiation is given by

$$\mathbf{a} = \frac{P_\perp \mathcal{E}}{mc}\,\mathbf{n}\;, \tag{1}$$

where $\mathcal{E}$ is the solar–radiation flux, m body's mass and c the light velocity. Part of the absorbed radiation is physically reprocessed in the body and later reemitted in the infrared band ("thermal radiation of the body"). The recoil force/acceleration due to this radiation field, also called Yarkovsky effect, has been extensively studied in the past years (e.g. Rubincam 1995, 1998; Vokrouhlický 1998a,b, 1999; Vokrouhlický et al. 2000) and it is not a subject of this paper. The complementary part of the absorbed radiation, a fraction given by the albedo coefficient A, is immediately re–radiated by the surface of the body. The recoil force/acceleration due to this reflected radiation is considered in this paper and will be evaluated under specified assumptions in the next two sections. For sake of simplicity we shall always assume the Lambert law of reflection of the body's surface (sometimes also called isotropic law in other contexts). It is well known that this assumption is not exactly satisfied for cosmic bodies, e.g., with the so called "opposition spike", but generalization of the results for non–Lambert reflection laws is beyond the scope of this paper.

There are two main factors resulting in a non constant recoil force/acceleration due to the reflected radiation: (i) variations in the albedo distribution over the surface, and (ii) non spherical shape of the body. Both factors will be illustrated in the next two sections. However, to keep the formulation of the problem comparatively simple and to be able to give exact analytical formulae for the resulting perturbations, we shall discuss only axisymmetric bodies. Of course real bodies would rotate, and provided their rotation period is short with respect to the orbital period we can consider a rotation–averaged shape and a rotation-averaged albedo, by definition axisymmetric, as a good approximation for the purpose of computing these radiation effects.

2.1. Anisotropic albedo distribution

In this section we give the recoil force/acceleration due to the reflected radiation on a spherical body with non constant but axially symmetric distribution of the albedo. In particular, we shall assume albedo modes that have an odd–symmetry with respect to the equator of the body since these have more important orbital effects than the even–symmetry terms (see below). A generic albedo distribution has then the following form: $A(\theta) = a_0 + a_k \cos^k \theta$ with an arbitrary odd–number k. Here, a_0 and a_k are constants and θ is the colatitude measured from the symmetry axis $\mathbf{s}$ (not necessarily identical with the rotation axis). A linear combination of such terms in $A(\theta)$ would just mean a linear combination of the perturbations, in a first order perturbative theory such as the one we are using, thus we shall assume the above description of the albedo distribution with k and odd integer and a_k an arbitrary constant.

The body–fixed frame direction $(-\mathbf{n})$ towards the Sun is given by the colatitude θ_0 (measured from the symmetry axis; $\cos\theta_0 = -\mathbf{n}\cdot\mathbf{s}$) and the longitude $\phi_0 = 0$ (defining the origin of the longitude ϕ along the body's equator). Let us also define the surface insolation function $I(\theta, \phi; \theta_0)$, yielding the flux of solar radiation absorbed by the surface element dS at (θ, ϕ) coordinates (with respect to the symmetry axis and the chosen origin of longitudes). Then, $I(\theta, \phi; \theta_0) = -(\mathbf{n}.\mathbf{n}_\perp)$ if positive, otherwise zero, with $\mathbf{n}_\perp$ the unit vector orthogonal to the surface of the body at (θ, ϕ), e.g., $\mathbf{n}_\perp = (\sin\theta\cos\phi, \sin\theta\sin\phi, \cos\theta)^T$ for a spherical body. In the development (e.g. Vokrouhlický 1998b)

$$I(\theta, \phi; \theta_0) = \sum_{n\geq 0} i_n(\theta, \theta_0)\, \cos n\phi \; , \tag{2}$$

the first two coefficients are

$$i_0(\theta; \theta_0) \; = \; \frac{2}{\pi} \left(\phi_\star \cos\theta \cos\theta_0 + \sin\phi_\star \sin\theta \sin\theta_0\right) \; , \tag{3}$$

$$\begin{aligned} i_1(\theta; \theta_0) \; &= \; \frac{1}{\pi} \Big[2 \sin\phi_\star \cos\theta \cos\theta_0 \\ &\quad + \left(\phi_\star + \sin\phi_\star \cos\phi_\star\right) \sin\theta \sin\theta_0 \Big] \; ; \end{aligned} \tag{4}$$

where the auxiliary angle $\phi_\star$ is defined by

$$\begin{aligned} \cos\phi_\star(\theta, \theta_0) \; &= \; -1 && \text{for } \theta < \theta_- \\ &= \; -\mathrm{ctg}\theta \,\mathrm{ctg}\theta_0 && \text{for } \theta \in (\theta_-, \theta_+) \\ &= \; 1 && \text{for } \theta > \theta_+ \end{aligned} \tag{5}$$

with $\theta_\pm = \frac{\pi}{2} \pm \theta_0$.

Assuming the reflection from the surface follows Lambert diffusion law, the recoil force acting upon each surface element is given by Milani et al. (1987), formula (4.7). Thus the recoil acceleration $\mathbf{a}'$ due to the reflected radiation on the entire body can be expressed in integral form

$$\mathbf{a}' = -\frac{2}{3}\frac{\mathcal{E}}{mc} \int A(\theta)\, I(\theta, \phi; \theta_0)\, \mathbf{n}_\perp \, dS \; , \tag{6}$$

with the integration assumed over the whole sphere and $dS = R^2\, d(\cos\theta)\, d\phi$ (R is the radius of the body). Assuming the simple albedo distribution $A(\theta)$ introduced above, the formula (6) may be integrated analytically. Adding the absorption radiation pressure term (1) with $P_\perp = \pi R^2$ for a sphere we obtain the total radiation acceleration

$$\begin{aligned} \mathbf{a}_1 \; = \; \kappa \left(1 + \frac{4}{9}\, a_0\right) \mathbf{n} + \kappa' \Big[& \cos\theta_0\, M_k(\theta_0)\, \mathbf{n} \\ & - \left(k \cos^2\theta_0\, M_k(\theta_0) + \sin^{k+1}\theta_0\right) \mathbf{s} \Big] \end{aligned} \tag{7}$$

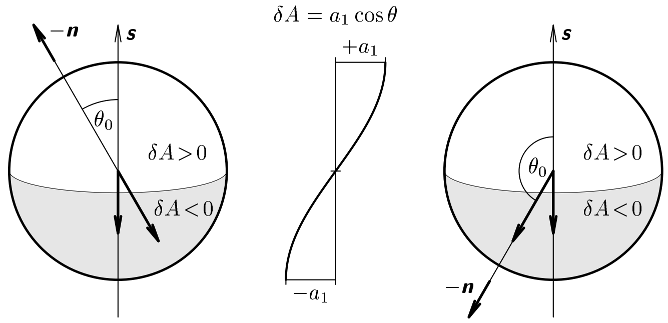

Fig. 1. Geometry of the solar radiation force on a spherical body with an axially symmetric distribution of albedo. The left panel shows the situation of $\theta_0 < \pi/2$ (θ_0 is the angle between the local direction to the Sun and the symmetry axis $\mathbf{s}$), the right panel shows the case of $\theta_0 > \pi/2$. The arrows indicate the directions along which the body is accelerated (see the second term in the formula (7)).

where

$$\kappa \; = \; \frac{\pi R^2 \mathcal{E}}{mc} = \frac{3}{4}\frac{\mathcal{E}}{\rho R c} \; , \tag{8}$$

$$\kappa' \; = \; \frac{4}{3}\, a_k\, \kappa\, \frac{k!!}{(k+3)!!} = \frac{a_k \mathcal{E}}{\rho R c}\, \frac{k!!}{(k+3)!!} \; , \tag{9}$$

and the functions $M_k(\theta_0)$ satisfying recurrence relations $(k = 1, 3, 5, \ldots)$

$$k\, M_k(\theta_0) = \sin^{k-1}\theta_0 + (k-1)\, M_{k-2}(\theta_0) \; , \tag{10}$$

initiated by $M_1(\theta_0) = 1$. The last expressions in Eqs. (8) and (9) assume a spherical body with average density ρ; of course for a real body the density would be poorly known. Note that the first term in the formula (7) is the usual acceleration of a spherical body with homogeneous albedo a_0. As it will be pointed out below, this term has little importance since it can only result in short–periodic orbital effects. The second term in (7) is due to the axially symmetric albedo term $\propto a_k \cos^k \theta$ and has much more important orbital effects (even though a_k is expected to be significantly smaller than a_0), as discussed in Sec. 2.3. A similar result for the specularly reflecting surface has been derived by Métris et al. (1997).

For $k = 1$, dipole asymetry of the albedo distribution, the formula (7) simplifies to

$$\mathbf{a}_1 = \kappa \left(1 + \frac{4}{9}\, a_0\right) \mathbf{n} + \kappa' \left(\cos\theta_0\, \mathbf{n} - \mathbf{s}\right) . \tag{11}$$

In what follows, we shall use this case to exemplify the dynamical effects of the albedo asymetry.

Figure 1 shows the geometry of the radiation pressure acceleration (7); this will help in understanding the long–term orbital effects. Note that for $a_k > 0$ the component along the symmetry axis ($\propto \mathbf{s}$) is always opposite to the unit vector defining the origin of colatitude, $\mathbf{s}$ and that the component in the solar direction ($\propto \mathbf{n}$) has a different orientation for $\theta_0 < \pi/2$ and for $\theta_0 > \pi/2$.

2.2. Ellipsoidal–shape bodies

In this section we shall investigate the effect of non–sphericity of the body and evaluate the radiation force/acceleration due to the reflected sunlight. Unlike in the previous section, we shall assume a constant albedo a_0, but we shall consider bodies of a ellipsoidal shape, with two equal axes (to maintain axial symmetry). The ratio of the polar (R_p) and the equatorial (R_e) radii will be denoted $\epsilon = R_p/R_e$. In principle this parameter may acquire an arbitrary value in the range $(0, \infty)$, being smaller than unity for oblate ellipsoids and larger than unity for prolate ellipsoids; but of course for rotating bodies $\epsilon < 1$.

In what follows we shall use the mathematical formulation of Vokrouhlický (1998b; see the Appendix of this paper for details). In particular, we shall not introduce the ellipsoidal coordinates, but rather keep parameterizing the surface elements dS, normal vectors $\mathbf{n}_\perp$ and other quantities by spherical polar coordinates (θ, ϕ) as before: θ is measured from the symmetry axis $\mathbf{s}$ of the body and the ϕ measured from an arbitrary origin at the equator (to be specified later).

The radiation pressure due to the absorbed sunlight is still given by Eq. (1), where the geometric cross–section $P_\perp$ is given by

$$P(\theta_0) = \pi R_e^2 \, J_2(\theta_0) \; , \tag{12}$$

where we have again assumed the Sun direction at an angle θ_0 from the symmetry axis, and where, following Vokrouhlický (1998b), we introduce the auxiliary functions $J_n(x)$ ($n = 1, 2, 3, \ldots$) by

$$J_n(x) = \sqrt{\epsilon^n \sin^2 x + \cos^2 x} \; . \tag{13}$$

Interestingly, when evaluating the radiation force/acceleration due to the reflected sunlight we may follow the formulation used in the previous Section provided the corresponding variables are generalized to depend on the parameter ϵ. In particular, the integral formula (6) is valid, provided the following changes are made:

– the surface element dS on the spheroid is given by

$$dS = \epsilon^2 R_e^2 \frac{J_4(\theta)}{J_2^4(\theta)} \, d(\cos\theta) d\phi \; , \tag{14}$$

– a unit vector normal to the surface element at colatitude θ and longitude ϕ is given by

$$\mathbf{n}_\perp(\theta, \phi) = \frac{1}{J_4(\theta)} \begin{pmatrix} \epsilon^2 \sin\theta \cos\phi \\ \epsilon^2 \sin\theta \sin\phi \\ \cos\theta \end{pmatrix} \; , \tag{15}$$

– the coefficients i_n of the insolation function $I(\theta, \phi; \theta_0)$ (we again assume $\phi_0 = 0$ for the solar longitude) are given by

$$i_0(\theta;\theta_0) \;=\; \frac{2}{\pi} \left(\phi_\star \cos\theta \cos\theta_0 + \epsilon^2 \sin\phi_\star \sin\theta \sin\theta_0 \right) \; , \tag{16}$$

$$\begin{aligned} i_1(\theta;\theta_0) \;=\; & \frac{1}{\pi} \Big[2 \sin\phi_\star \cos\theta \cos\theta_0 \\ & + \epsilon^2 \left(\phi_\star + \sin\phi_\star \cos\phi_\star \right) \sin\theta \sin\theta_0 \Big] \; , \end{aligned} \tag{17}$$

with the angle $\phi_\star$ reading

$$\begin{aligned} \cos\phi_\star(\theta, \theta_0) \;&=\; -1 && \text{for } \theta < \theta_- \\ &=\; -\epsilon^{-2} \, \mathrm{ctg}\theta \, \mathrm{ctg}\theta_0 && \text{for } \theta \in (\theta_-, \theta_+) \\ &=\; 1 && \text{for } \theta > \theta_+ \end{aligned} \tag{18}$$

and $\mathrm{ctg}\theta_\pm = \mp \epsilon^2 \mathrm{tg}\theta_0$.

These formulae generalize the corresponding variables from Sec. 2.1 for the $\epsilon \neq 1$ case.

Assuming $A(\theta) = a_0$ in Eq. (6), that is constant albedo, we can still obtain an analytic result for the total radiation acceleration of the ellipsoidal body in the form

$$\mathbf{a}_2 \;=\; \kappa \left\{ \left[J_2\left(\theta_0\right) + \frac{4}{9} a_0 \psi_{_X}\left(\epsilon\right) \right] \mathbf{n} - \frac{4}{9} a_0 \psi_{_{ZX}}\left(\epsilon\right) \cos\theta_0 \, \mathbf{s} \right\} \; , \tag{19}$$

where we keep the notation of Vokrouhlický (1998b)

$$\psi_{_X}\left(\epsilon\right) \;=\; \frac{3}{4} \frac{\epsilon^2}{\eta^2} \left[\frac{1+\eta^2}{2\eta} \ln\left(\frac{1+\eta}{1-\eta} \right) - 1 \right] \; , \tag{20}$$

$$\psi_{_Z}\left(\epsilon\right) \;=\; \frac{3}{2\eta^2} \left[1 - \frac{\epsilon^2}{2\eta} \ln\left(\frac{1+\eta}{1-\eta} \right) \right] \tag{21}$$

where $\eta = \sqrt{1-\epsilon^2}$ and $\psi_{_{ZX}}(\epsilon) = \psi_{_Z}(\epsilon) - \psi_{_X}(\epsilon)$ (see Figure 1 in Vokrouhlický 1998b for the functional dependence of the ψ–functions on the oblateness parameter ϵ). The amplitude κ is given by (8) provided the radius R is replaced by the equatorial radius R_e of the spheroid in the second term and the polar radius R_p in the last term (this approximation corresponds again to a body with constant density). Note that in the case of prolate ellipsoids ($\epsilon > 1$) η becomes imaginary; in this case we can use the following identity, holding for any complex number z ($i = \sqrt{-1}$ is the complex unit):

$$\ln[(1+z)/(1-z)] = -2 \, i \, \mathrm{arctg}(iz) \; . \tag{22}$$

Taking the limit $\epsilon \rightarrow 1$ we note that $J_2(\theta_0) \rightarrow 1$, $\psi_{_X} \rightarrow 1$ and $\psi_{_{ZX}} \rightarrow 0$, and Eq. (19) thus extends the usual formula for the radiation pressure on a spherical body. As expected, when $\epsilon \neq 0$ a symmetry–axis–aligned ($\propto \mathbf{s}$) acceleration components occurs with "seasonal" modulation due to the $\cos\theta_0$. See Figure 2 for a geometric insight.

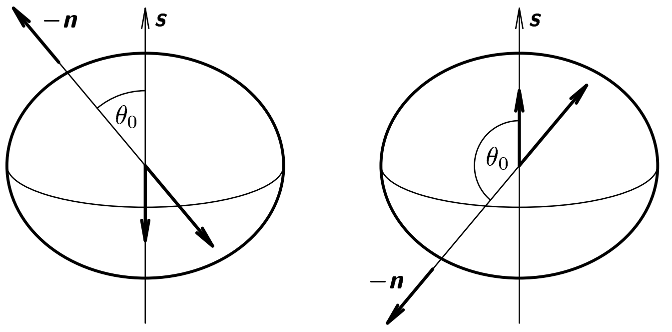

Fig. 2. Geometry of the solar radiation force on a spheroidal body with $\epsilon < 1$. The left panel shows the situation of $\theta_0 < \pi/2$ (θ_0 is the angle between the local direction to the Sun and the symmetry axis $\mathbf{s}$), the right panel shows the case of $\theta_0 > \pi/2$. The arrows indicate the directions along which the body is accelerated (see the formula (19)).

2.3. Poynting–Robertson effect

We recall here the perturbing acceleration due to the Poynting–Robertson effect but we shall not rederive the corresponding formulae. They can be found in textbooks (e.g. Bertotti & Farinella 1990) or journal reviews (e.g. Burns et al. 1979).

The PR acceleration of a spherical body with constant surface albedo a_0 is given by

$$\mathbf{a}_3 = -\frac{\kappa}{c}\left(1+\frac{4}{9}a_0\right)\left[\mathbf{v}+(\mathbf{v}.\mathbf{n})\mathbf{n}\right] , \qquad (23)$$

where κ is the same radiation factor from (8), c is the speed of light, $\mathbf{v}$ the orbital velocity vector and $\mathbf{n}$ the unit vector of the asteroid heliocentric position.

2.4. Long–term orbital effects

As a first glimpse to understand the orbital perturbations due to the radiation forces (11) and (19) we compute the orbit averaged values of the semimajor axis (a), eccentricity (e) and inclination (I) perturbation rate. Note that none of these elements undergoes long–term perturbations in the case of the radiation force acting on a spherical body with constant albedo. Only the new features (zonal albedo variations or non-spherical shape) yield such perturbations and thus their effect can accumulate with time and lead to observable effects. To compute these long term perturbations we proceed by using the averaging principle (Milani et al. 1987, Section 3.4), which allows to compute them (to first order in the perturbation small parameters) by averaging the perturbation equations over one orbit. When performing this averaging we should not overlook that the solar radiation flux $\mathcal{E}$ in Eqs. (8) and (9) decreases with square of the distance from the Sun; $\mathcal{E} \propto 1/r^2$. In fact this effect makes the averaging simpler, since it makes easier to transform to the true anomaly as the integration variable.

Including the radiation force (11) into the Gauss equations an taking the average over one revolution we obtain (no truncation in eccentricity)

$$\frac{da}{dt} = -\frac{3\kappa_a'}{n}\, s_Q\, \frac{e}{\beta^2} , \qquad (24)$$

$$\frac{de}{dt} = -\frac{\kappa_a'}{2na}\, s_Q\, \frac{3+5\beta}{1+\beta} , \qquad (25)$$

$$\frac{dI}{dt} = \frac{\kappa_a'}{na}\, s_c\, \frac{e\cos\omega}{\beta(1+\beta)} , \qquad (26)$$

with $\beta = \sqrt{1-e^2}$, n mean motion and ω the longitude of pericenter. The index a in the quantity κ' indicates that the radiation flux $\mathcal{E}$ in κ is to be evaluated at a distance from the Sun equal to the semimajor axis a. The scalar quantities s with different indexes denote projection of the symmetry axis $\mathbf{s}$ onto different, orbit–defined directions: $s_P = \mathbf{s}\cdot\mathbf{P}$ ($\mathbf{P}$ in the direction of the pericenter), $s_c = \mathbf{s}\cdot\mathbf{c}$ ($\mathbf{c}$ in the direction of the orbital angular momentum; hence s_c is cosine of the obliquity angle), $s_Q = \mathbf{s}\cdot\mathbf{Q}$ ($\mathbf{Q} = \mathbf{c}\times\mathbf{P}$).

Similarly, including the acceleration term (19) in Gauss equations and taking the average over one orbit we obtain

$$\frac{da}{dt} = 0 , \qquad (27)$$

$$\frac{de}{dt} = -\frac{4}{9}\, a_0\, \frac{\kappa_a}{na}\, \psi_{zx}(\epsilon)\, \frac{e\beta}{(1+\beta)^2}\, s_P s_Q , \qquad (28)$$

$$\frac{dI}{dt} = \frac{4}{9}\, a_0\, \frac{\kappa_a}{na}\, \psi_{zx}(\epsilon)\, \frac{s_c}{1+\beta}\left[s_a + (1-\beta)\, s_Q \sin\omega\right] , \qquad (29)$$

with the same notation as before and $s_a = \mathbf{s}.\mathbf{a}$, with $\mathbf{a}$ being the unit vector along the line of node.

A few comments are in order. First, the most important feature of the long–term orbital perturbation due to the odd–symmetry albedo variation is the semimajor axis drift (24). This effect results in the orbit displacement that accumulates quadratically with time, compared to the linear perturbations due to the eccentricity and inclination effect. It is easy to check that the even–symmetry zonal albedo terms do not yield this effect. To be precise we mention that the semimajor axis effect (24) is not secular in a strict sense, but long–periodic, since the $\mathbf{Q}$–vector typically undergoes a long–term circulation. This effect may be, however, neglected if we are interested in NEA orbit displacement during less than one century (typical node and perihelion precession periods are of the order of $10^3 - 10^5$ years). We also note that the semimajor axis effect disappears for circular orbits ($e = 0$) which, however, is not the case for NEA orbits, typically with high e. Figure 3 should help in understanding the long–term semimajor axis effect discussed above, at least for the case $\mathbf{s} = \mathbf{Q}$, that is with the symmetry axis in the orbital plane, orthogonal to the line of apsides.

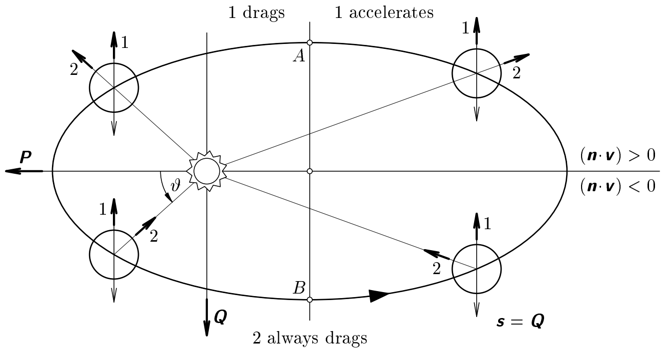

Fig. 3. The net long periodic semimajor axis drift due to the odd–symmetry zonal term in the albedo distribution (see also Figure 1). The symmetry axis ($\propto \mathbf{s}$) acceleration component 1 contributes to a drag over half of the orbital period (over the arc APB) while anti–drags over the complementary half of the orbital period. The scalar product of the radial ($\propto \mathbf{n}$) acceleration component 2 and the osculating velocity is always negative for an elliptic orbit, resulting thus in net drag (for $a_k > 0$): thus in the long run this is the dominant effect.

Eq. (27) indicates that the orbit–averaged drift of the semimajor axis is zero (for orbits of arbitrary eccentricity) for radiation forces acting on spheroidal objects of constant albedo. We may thus assume that the orbit–displacement would smaller than in the previous case, thus difficult to observe. We shall verify this conclusion in Sec. 3 below.

For the PR effect we remind the classical formulae, originally obtained by Wyatt & Whipple (1950), for the secular effects in the semimajor axis and the eccentricity (no inclination effect)

$$\frac{da}{dt} = -\kappa_a \left(1 + \frac{4}{9}a_0\right) \frac{a}{c} \frac{3 + 2e^2}{(1-e^2)^{3/2}} , \tag{30}$$

$$\frac{de}{dt} = -\frac{5\kappa_a}{2c} \left(1 + \frac{4}{9}a_0\right) \frac{e}{(1-e^2)^{1/2}} , \tag{31}$$

$$\frac{dI}{dt} = 0 . \tag{32}$$

A more thorough treatment of the PR orbital effects has been recently given by Breiter & Jackson (1998), but the approximation above is accurate enough for our purpose.

3. Examples

We illustrate the theory of the orbit perturbations due to the radiation effects, as formulated in the previous sections, with two examples, namely two near–Earth asteroids: 6489 Golevka and 1566 Icarus. These objects have been found potentially interesting targets for detection of the Yarkovsky effect (Vokrouhlický et al. 2000). The orbital eccentricity is large in both cases, 0.599 and 0.827, which suggests the possibility of large long–term orbital changes according to the formulas given in this paper, especially (24).

The technique used in this text is fairly similar to that in Vokrouhlický et al. (2000), but we add a preliminary step in the analysis to obtain a first information about the orbit displacement produced by presence of the radiation forces in the dynamical model. At this stage we disregard planetary and more subtle (e.g., relativistic) perturbations of the asteroid orbit and consider the solar gravitational influence and the radiation forces only ("perturbed two–body problem").

Given the initial orbital elements at an epoch corresponding to the weighted mean of the available observations, we numerically integrate the asteroid orbit with the radiation forces (7), (19) and/or (23) included in the model. We readjust the initial orbital elements to match the integrated orbit by a Keplerian ellipse in the sense of the least squares technique. Residuals after this fitting procedure give an information about the "true" order of magnitude of the radiation–effect perturbations (keeping the initial elements unchanged the residuals would be polluted by unobservable free–Keplerian terms).

Since the radar ranging yields the most precise observations, we project the orbit perturbation onto the geocentric line–of–sight direction of the asteroid. We thus obtain the perturbation of the geocentric distance ΔR and of the corresponding rate $d\Delta R/dt$. The first is related to the radar delay measurement and the second to the Doppler shift between the transmitted and received signal. At this stage of our procedure we also check validity of the formulae (24) – (26) and (27) – (29) for the long–term effects in the Keplerian elements.

At the second, and a more precise, stage we use the `OrbFit` program that allows the orbit determination from the optical and radar astrometry data. An information about this software, and a free download, may be obtained from http://newton.dm.unipi.it/˜asteroid/orbfit/. We proceed in exactly the same way as in Vokrouhlický et al. (2000); a complete dynamical model to the post–Newtonian level is used for the orbit determination from the available data. For the given asteroid, the initial state vector and the covariance matrix constructed at the weighted mean of the observations is propagated to the next close approach to the Earth (when the radar observation might be taken). The $\sigma = 3$ confidence region, as determined by the fit to the current data, is projected onto the space of the radar observables, notably distance from the Earth and rate of change of this quantity (with aberration effects and other small corrections included). This projection is performed with the algorithms discussed in Milani (1999) and implemented in `OrbFit` both for optical astrometry and radar astrometry. Such projection is constructed for two models: (i) a "nominal" model, not including the solar radiation perturbation, and (ii) an "extended" model, including the solar radiation perturbation. Position of the confidence regions predicted by the two

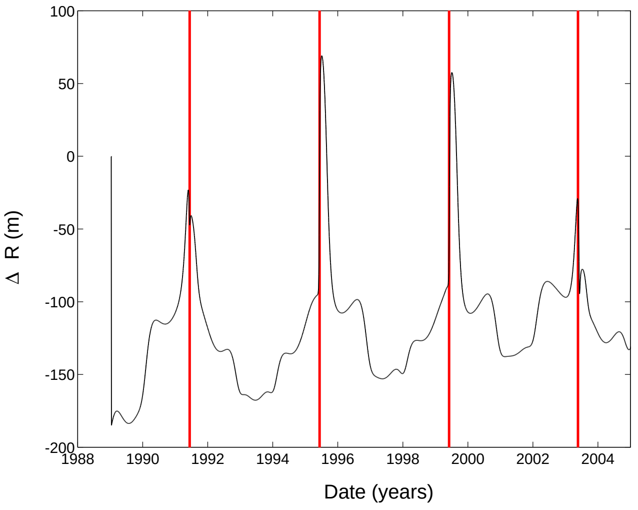

Fig. 4. Simulated orbit displacement ΔR along the line–of–sight from the Earth for the asteroid 6489 Golevka vs time between 1988 and 2006. An odd–symmetry zonal term $\propto 0.01 \cos\theta$ of the Golevka's albedo assumed (i.e. $k = 1$, $a_1 = 0.01$ in the text). Radius ($R = 265$ meters) and the spin axis $\mathbf{s}$ orientation from Hudson et al. (2000). The four close approaches to the Earth denoted by shaded strips.

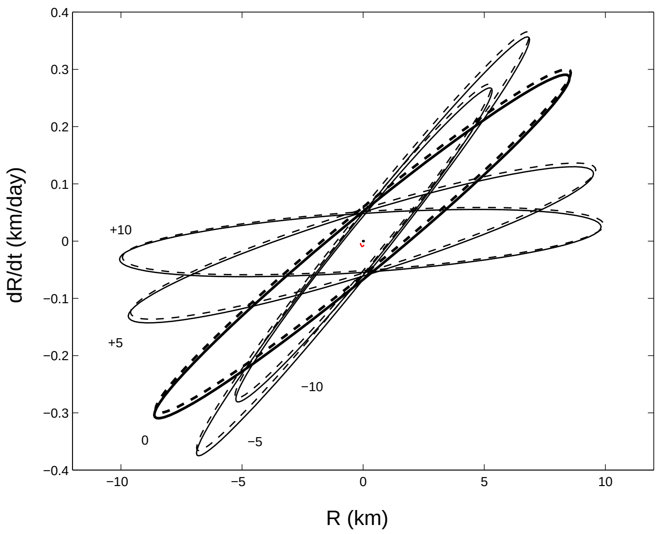

Fig. 5. Projection of the 3σ confidence ellipses of the Golevka orbit uncertainty onto the space of radar observables: the geocentric distance R (in km) and the rate–of–change of the geocentric distance dR/dt (in km/day). Results of the nominal model (without the radiation effects) given by the dashed lines, while results of the extended model (including the radiation effects) given by the solid lines. Origin of axes referred to the corresponding values of the nominal model. Data at the nearest future close approach of Golevka (20 May, 2003) are given by thick lines. Similar results 5 and 10 days before and after the close approach of the nominal orbit are shown by the lighter curves with labels ± 5 and ± 10. The extended model is obtained by adding an odd–symmetry zonal term $\propto 0.01 \cos\theta$ in the albedo of Golevka (i.e. $k = 1$, $a_1 = 0.01$ in the text). Radius ($R = 265$ meters) and spin axis $\mathbf{s}$ orientation from Hudson et al. (2000).

models is compared. When no overlapping at the $\sigma = 3$ level is observed, we can conclude that the radiation effects might be detected during the next close approach of the asteroid. If the two confidence regions partially overlap, we can evaluate the probability (less then unity) of this detection.

The results obtained with the less accurate perturbed two body method method are consistent, as far as the size of the perturbations is concerned, with the results obtained with the more accurate procedure. This implies that nonlinear coupling of the radiation forces with gravitational perturbations is not important, at least over time spans of the order of tens of years.

3.1. Golevka

Golevka has been observed by radar in June 1991, 1995 and 1999. Unfortunately, the 1999 data cannot be used as astrometric data; thus the 91–95 baseline is rather short to detect subtle non–gravitational phenomena in Golevka's orbit. Nevertheless, the next close approach to the Earth occurs on May 20, 2003. Vokrouhlický et al. (2000) considered the possibility to detect the Yarkovsky perturbation using the radar data which we presume will be taken at this approach. Here we are going to investigate whether these data could reveal existence of the direct solar radiation pressure perturbations on the orbit of Golevka.

We consider the physical parameters of Golevka as derived by Hudson et al. (2000): notably surface albedo (a_0) of 0.15, mean radius of 265 meters and spin axis orientation $\mathbf{s}$ with ecliptic longitude and latitude $\ell = 202^0$ and $b = -45^0$. These values superseed the previous model of Golevka by Mottola et al. (1997) and is consistent with indications Zaitsev et al. (1997). The shape model of Golevka, as derived from the radar observations, is very complex and impossible to fit with a ellipsoidal model (to which our theory is limited). We can only obtain an order of magnitude of the non–sphericity effect by adopting $\epsilon \simeq 0.8$, a rather conservative value since the estimate of the longest to shortest geometric axes of Golevka is about 1.4 (Hudson et al. 2000).

In the first step, we use the perturbed two-body formulation discussed above. Figure 4 shows the the orbit perturbation for Golevka projected onto the geocentric line–of–sight for the effect of variable albedo (acceleration $\mathbf{a_1}$ from (7); note that the absorbed radiation pressure effect – the first term in (7) – is also included). We have assumed $k = 1$ and $a_1 = 0.01$, which means a 2% difference of the albedo values between the southern and the northern hemisphere. Such a small albedo variation cannot be measured from the Golevka lightcurve data. In fact, Magnusson (1991) indicates that smaller asteroids show in average larger variation of the surface albedo. Thus the value $a_1 = 0.01$ adopted in this text seems to be a conservative estimate. Nevertheless, the dynamical effect is rather large – up to 150 meters during the 1995 close approach. Moreover, the effect accumulates with time so that the perturbation with still increase in the future. Notice the rapid change in the sign of the range perturbation during the close approaches (especially in 1995). A typical time scale of this change is $\simeq$ 40 days. During the 1995 closest approach time the perturbation is close to zero. Since the observations cover only about 12 days around the close approach (and only 10 days in 1991), the maxima of the perturbation in range might not be covered by the observations. In 2003, the close approach perturbation is somewhat smaller, about 75 meters. This value is larger than the uncertainty of the observations (of the order of 40 meters), but smaller that the orbit determination uncertainty from the current data (about 8.5 km).

The results of the simpler model are confirmed by the analysis of the complete solution shown in the Figure 5. The projection of the 3σ uncertainty ellipsoid onto the plane of the radar observables, range R and range–rate dR/dt, is shown for two models: (i) the nominal model that do not include the radiation effects (dashed lines), and (ii) the extended model that includes the $\mathbf{a}_1$ acceleration (solid lines). The axes origin always referred to the nominal–model solution. The same parameters of the albedo anisotropy as above. The thicker lines indexed 0 correspond to the time of the closest approach of the nominal orbit (20 May, 2003). Similar confidence boundaries for five and ten days before and after this data are shown by thinner lines, labeled ± 5 and ± 10. The confidence levels are computed from the least squares fit to the currently available astrometric data (both optical and radar). Note that the mean displacement of about hundred meters is in a good agreement with the previous simpler analysis. However, the rather large orbit uncertainty prevents detection of the radiation effect: the uncertainty regions overlap to a large extend. We have checked that the results are not much sensitive on the degree k of the albedo distribution, provided k is not too large.

Figure 6 shows the result of the perturbed two–body approach for the radiation pressure on a flattened Golevka ($\mathbf{a}_2$ acceleration from (19)). A constant albedo of 0.15 is assumed, and the flattening parameter $\epsilon = 0.8$ as discussed above. The effect is smaller, but comparable, to the perturbation due to the radiation pressure on a spherical body with variable albedo (above). In Figure 6 we have assumed that the Golevka's spin axis $\mathbf{s}$ is fixed in space. However, we have verified that free precession with a cone aperture up to 15 degrees does not change our conclusions. We do not report the PR effect perturbation of the Golevka's orbit, since it is quite small (smaller than 5 meters in range variation).

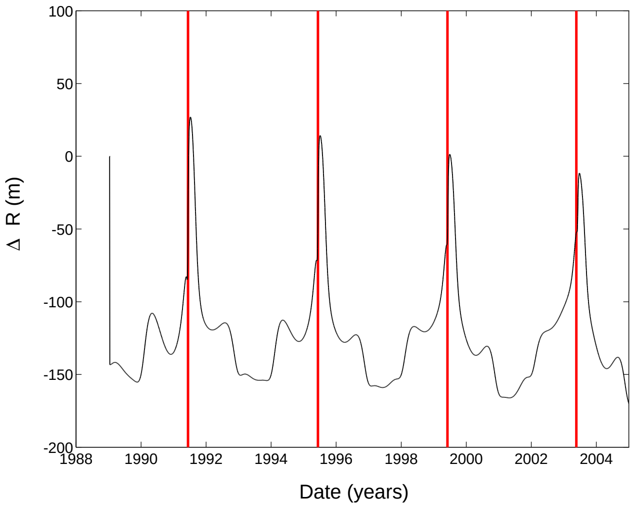

Fig. 6. Simulated orbit displacement ΔR along the line–of–sight from the Earth for the asteroid 6489 Golevka vs time between 1988 and 2006. Golevka is approximated with a spheroid with oblateness parameter $\epsilon \simeq 0.8$ and polar radius $R_p = 212$ meters. A constant surface albedo $a_0 = 0.15$ is assumed, and the spin axis $\mathbf{s}$ orientation from Hudson et al. (2000). The four close approaches to the Earth are denoted by shaded strips.

In general, we can conclude that though larger than the observation uncertainty, the radiation effects could hardly be detectable from the radar data taken during the next close approach. The main reason is a too short observed time span (the 1988–2003 interval covers little more than 4 revolutions of the asteroid around the Sun). Thus the effect of the long periodic perturbations in a and e thus cannot accumulate to large orbit displacements. In both cases reported above, the short periodic effect due to the elementary radiation pressure (purely radial force) contributes largely to the perturbation.

3.2. Icarus

Icarus is the first asteroid observed by the radar technique (June 1968). It has been also observed at the next close approach to the Earth in June 1996 and returns back in June 2015. These dates define a suitably long time span over which we have a good quality orbital data (despite the fact that all radar data available so far are Doppler measurements only). Moreover, Icarus' high eccentricity (0.827) results in high rates of long term drifts in the element, especially a, as it is clear from (24). For that reason Vokrouhlický et al. (2000) considered a possibility to de-

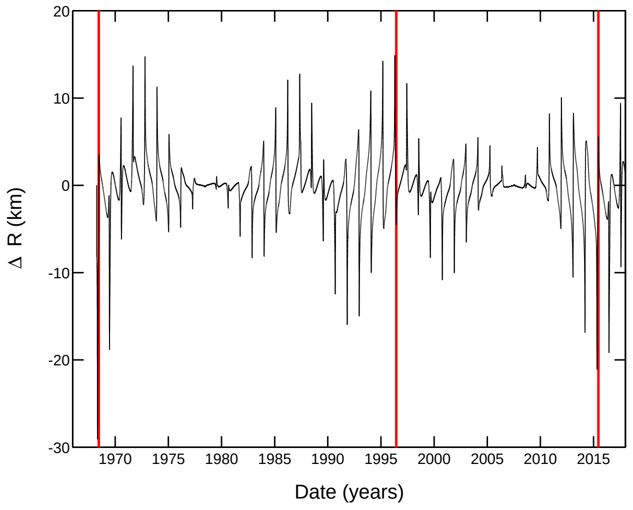

Fig. 7. Simulated orbit displacement ΔR along the line–of–sight from the Earth for the asteroid 1566 Icarus vs time between 1966 and 2018. An odd–symmetry zonal term $\propto 0.01\cos\theta$ is assumed in the albedo of Icarus (i.e. $k=1$, $a_1=0.01$ in the text). The radius ($R=450$ meters) and the spin axis $\mathbf{s}$ orientation are taken from De Angelis (1995). The three close approaches to the Earth are denoted by shaded strips.

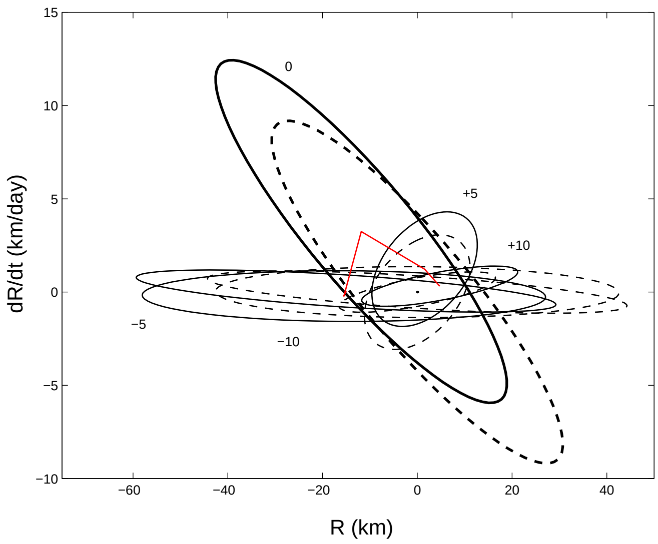

Fig. 8. Projection of the 3σ confidence ellipses of the Icarus orbit uncertainty onto the space of radar observables: the geocentric distance R (in km) and the range–rate dR/dt (in km/day). Results of the nominal model (without the radiation effects) given by dashed lines, while results of the extended model (including the radiation effects) are given by solid lines. The origin of the axes refers to the corresponding values of the nominal model. The results for the nearest future close approach of Icarus (16 June, 2015) are shown by thick lines. Similar results for 5 and 10 days before and after the close approach of the nominal orbit are shown by the lighter curves with labels ±5 and ±10. An odd–symmetry zonal term $\propto 0.01\cos\theta$ is assumed for the Icarus albedo (i.e. $k=1$, $a_1=0.01$ in the text). The radius ($R=450$ meters) and the spin axis $\mathbf{s}$ orientation are from De Angelis (1995).

tect the Yarkovsky effect in the motion of Icarus with he 2015 data. Here, we complement their analysis by the investigation of other radiation effects acting on the same orbit.

As for the physical data about Icarus we refer to the work of Veeder et al. (1989), De Angelis (1995) and Mahapatra et al. (1999). Veeder et al. give a radius of about 450 meters with a surface albedo of 0.4 (these values are used in this paper). Harris (1998) estimates a little larger radius ($\simeq 635$ meters) corresponding to a somewhat lower albedo, but reanalysis of the 1996 radar data by Mahapatra et al. (1999) supports Icarus' small size. De Angelis (1995) reports a triaxial shape model with ratios of the semi-axes $a/b\simeq1.23$ and $b/c\simeq1.4$. Since we cannot yet model the radiation effect on a triaxial ellipsoid we approximate Icarus' shape by a biaxial ellipsoid with a flattening parameter $\epsilon\simeq0.65$. The spin axis orientation parameters ($\ell=214^0$ and $b=5^0$) were taken from De Angelis (1995).

We again start our analysis by considering the perturbed two–body problem with the perturbation given by the radiation acceleration $\mathbf{a}_1$ from (7). The following parameters of the surface albedo anisotropy are assumed: $k=1$ and $a_1=0.01$. The 2% amplitude of the north/south asymmetry is very conservative and may even underestimate the real albedo variation. Figure 7 shows the perturbation of the geocentric distance to the asteroid. Contrary to the Golevka example, the perturbation is now much larger and is dominated by the secular effect in the semimajor axis due to the albedo asymmetry (the short–periodic effect of the absorbed radiation pressure is negligible). The 2015 range perturbation may be as large as 26 km, again with a rapid change during a time span of about one month around the closest approach. This perturbation is significantly larger than the expected observation uncertainty (Mahapatra et al. 1999), but little smaller than the current orbit uncertainty propagated to 2015. These facts indicate that the albedo variation effect might be important for precise analysis of the 2015 radar data. We also mention that the range–rate perturbation is smaller than the range perturbation. In both previous close approaches to the Earth (1968 and 1996) the maxima of the range–rate perturbation ($\simeq 3$ km/day) were either comparable or smaller than the formal uncertainty of the observations ($\simeq 4$ km/day for the 1968 observations and even 2 km/day for the 1996 observations).

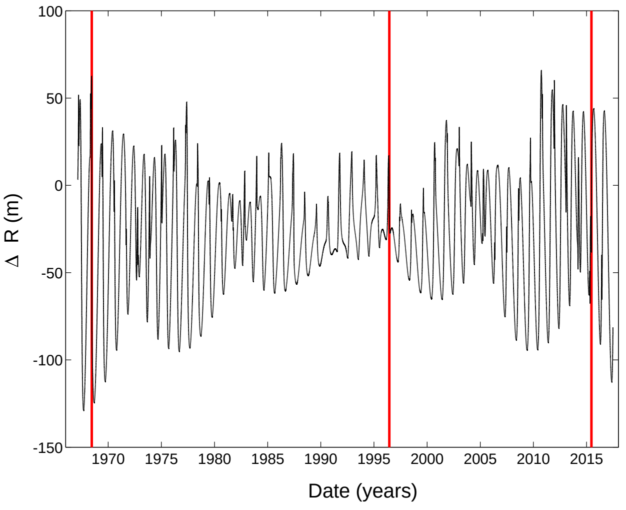

Fig. 9. Simulated orbit displacement ΔR along the line–of–sight from the Earth for the asteroid 1566 Icarus vs time between 1966 and 2018. Icarus is approximated with a spheroid with the oblateness parameter $\epsilon \simeq 0.65$ and the polar radius $R_p = 340$ meters. A constant surface albedo $a_0 = 0.4$ taken into account and the spin axis $\mathbf{s}$ orientation from De Angelis (1995). The three close approaches to the Earth denoted by shaded strips.

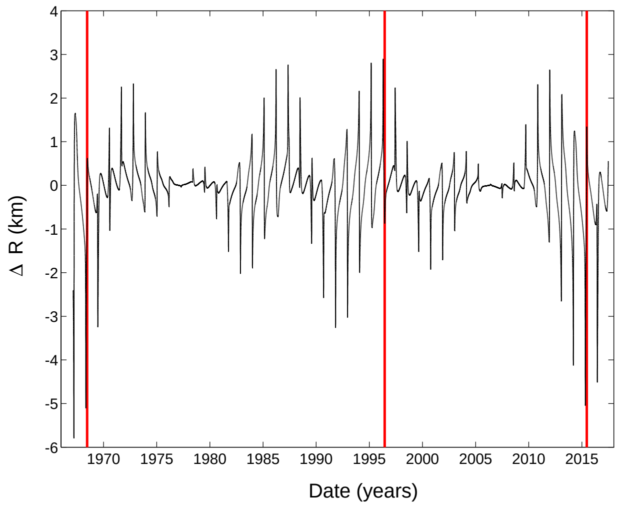

Fig. 10. Simulated orbit displacement ΔR along the line–of–sight from the Earth for the asteroid 1566 Icarus vs time between 1966 and 2018 due to the Poynting–Robertson effect. A radius $R = 450$ meters considered. The three close approaches to the Earth are denoted by shaded strips.

The importance of the perturbation due to the Icarus non uniform albedo is confirmed by the detailed analysis using the `OrbFit` program. Figure 8 shows the $\sigma = 3$ uncertainty ellipsoids projected onto the radar observables for the 2015 close approach of Icarus (dates before and after the close approach are also considered as before in the Golevka's case). Comparison of the nominal model (no radiation effects) and the extended model (including the perturbing acceleration $\mathbf{a}_1$ with the albedo asymmetry parameters as before) shows partial separation of the uncertainty ellipses. Though even in this case the radiation effect will not be possibly "detected" during the next close approach in 2015, it may potentially produce important orbit perturbation on a long–term because new radar data will potentially shrink the orbit determination uncertainty. We also note that the observed mean separation of the confidence intervals of the two models also confirms results of the simplified approach from the Figure 7.

Secondly, we consider the effect of Icarus' nonsphericity for the resulting radiation pressure – the acceleration (19). The flattening parameter ϵ are noted above. Figure 9 shows the geocentric range perturbation as results from the perturbed two–body analysis. The effect is very small, if compared to the non uniform albedo case studied above.

As a final example we consider the Icarus' orbit perturbation due to the Poynting–Robertson effect. Figure 10 shows the geocentric range perturbation within the perturbed two–body problem. Though smaller than in the Figure 7, the orbit displacement is still of an appreciable order of magnitude ($\simeq$ 5 km during the 2015 close approach). Surprisingly thus, the PR effect must be taken into account for the orbit analysis of Icarus including and beyond the 2015 approach, at least for consistency.

4. Conclusions

We give explicit, analytic formulas for the solar radiation dynamical effects on the orbits of Near–Earth Asteroids: this includes the radiation pressure due to the absorbed and reflected sunlight, not neglecting the (v/c)–correction. The effects of zonal albedo variations, with an odd–symmetry with respect to the equator, and of a biaxial ellipsoidal shape shape are considered. Both are interesting, since they produce long–term variations of the orbital elements which produce accumulation of the orbit perturbation.

For objects with observations spanning a long interval of time and with a high–eccentricity orbit, the dynamical effect of a non uniform albedo can result in a perturbation considerably larger than the other effects considered here. For instance, a conservative assumption about the north/south albedo asymmetry, too small to be detected from the photometry, results in multikilometer perturbation of the orbit of the NEA Icarus during the next close approach to the Earth. When analyzing the radar data which we presume will be taken during this future approach, one should pay a detailed attention to this effect. The perturbation due to the nonsphericity of Icarus shape are still larger then the observation uncertainty, but much smaller than the albedo effects. Our results also indicate a surprisingly large influence of the Poynting–Robertson effect.

We also remind that all perturbations studied in this paper are smaller than those due to the Yarkovsky effect, which is likely to remain the dominant radiation–related perturbation in the NEA orbits. Only for objects with very large north/south albedo asymmetry the direct radiation pressure effect (7) may exceed in magnitude the perturbation due to the Yarkovsky effect.

Since this paper only initiates the application of the radiation force dynamical effect for the NEA orbits, a number of approximations has been adopted. A further progress in removing these simplifications is desirable. For instance, generalization of the results presented in this paper for triaxial ellipsoids or objects of more complex shape may be an interesting extension of this work. Similarly, a more systematic analysis of the albedo variation effects (dropping out the assumption of the axial symmetry and isotropy of the sunlight reflection on the surface) might be another interesting extension of this work.

Acknowledgements. The authors thank M. Brož for help in drawing Figures 1 to 3 and to S.J. Ostro for giving access to the new physical model of the asteroid Golevka before publication. The `OrbFit` software is maintained by a consortium including the second author, M. Carpino, Z. Knežević and G.B. Valsecchi. The orbital data and the auxiliary information necessary for the orbit fit of Golevka and Icarus have been downloaded from the `NEODyS` online information system (`http://newton.dm.unipi.it/neodys/`). This research has been supported by grants PSN-1999-XXX and PSN-1999-XXX from the Italian Space Agency (ASI).

References

Bertotti B., Farinella P., 1990, *Physics of the Earth and the Solar System*, Kluwer Acad. Publ., Dordrecht
Breiter S., A.A. Jackson, MNRAS 299, 237
Burns J.A., P.L. Lamy, S. Soter, 1979 Icarus 40, 1
De Angelis G., 1995, Planet. Sp. Sci. 43, 649
Harris A.W., 1998, Icarus 131, 291
Hudson R.S., S.J. Ostro, R.F. Jurgens, et al., 2000, Radar observations and physical modeling of asteroid 6489 Golevka, Icarus, submitted
Magnusson P., 1991, A&A 243, 512
Mahapatra P.R., S.J. Ostro, L.A.M. Benner, et al., 1999, Planet. Space Sci. 47, 987
Métris G., D. Vokrouhlický, J.C. Ries, R.J. Eanes, 1997, J. Geophys. Res. 102, 2711
Milani, A., 1999, Icarus 137, 39
Milani, A., Nobili, A M., Farinella, P., 1987, *Non-gravitational perturbations and satellite geodesy*, Adam Hilger, Bristol.
Mottola S., A. Erikson, A.W. Harris, et al., 1997, AJ 114, 1234
Rubincam D.P., 1995, J. Geophys. Res. 100, 1585
Rubincam D.P., 1998, J. Geophys. Res. 103, 1725
Veeder G.J., M.S. Hanner, D.L. Matson, et al., 1989, AJ 97, 1211
Vokrouhlický D., 1997, Icarus 126, 293
Vokrouhlický D., 1998a, A&A 335, 1093
Vokrouhlický D., 1998b, A&A 338, 353
Vokrouhlický D., 1999, A&A 344, 362
Vokrouhlický D., P. Farinella, 2000, Nature, in press
Vokrouhlický D., A. Milani, S.R. Chesley, 2000, Yarkovsky effect on small near–Earth asteroids: mathematical formulation and examples, Icarus, in press
Williams J.G., X.X. Newhall, J.O. Dickey, 1996, Phys. Rev. D53, 6730
Wyatt S.P., F.L. Whipple, 1950, ApJ 111, 134
Zaitsev A.L., S.J. Ostro, S.P. Ignatov, et al., 1997, Planet. Sp. Sci. 45, 771

This article was processed by the author using Springer-Verlag LaTeX A&A style file *L-AA* version 3.